

MODELING OF STRUCTURAL VIBRATION FOR MOTOR CHAMBER INTERNAL FLOW STUDIES

D.R. Greatrix

Ryerson University, School of Aerospace Engineering
Toronto, Canada
greatrix@acs.ryerson.ca

V. Kudriavtsev

CFD Canada,
Toronto, Canada
vvk@cfdcanda.com

ABSTRACT

Axial, radial and tangential structural oscillation of various propulsion system motor chamber walls is demonstrated to be able to produce substantial pressure wave amplitudes within the internal flow. Predicted resonant driving frequencies for forced rigid vibration may vary somewhat from the ideal acoustic estimate, depending on the grid density employed in the given numerical model. Similarly, predicted limiting pressure wave amplitudes may tend to asymptote somewhat higher in the case of radial and tangential structural motion, as the grid density is increased (and the corresponding time step decreased) for the numerical solver. Free dynamic structural deformation (in addition to any net rigid-body motion that might be involved) is illustrated to also have an appreciable influence on internal gasdynamic wave behaviour.

INTRODUCTION

Severe structural vibration of propulsion system combustion chamber walls has been experimentally observed to appear in conjunction with symptoms commonly attributed to combustion instability.^{1,2} Propulsion systems affected by symptoms such as sustained axial and transverse pressure wave development and base pressure shifts (dc rise) include solid propellant rocket motors (SRMs), liquid propellant rocket engines (LREs), hybrid rocket engines (HREs), and jet engine afterburner sections. In the past, it has been common to assign such symptoms to a wholly combustion-related driving mechanism, e.g., augmented propellant burning rate as a function of a cyclic pressure wave presence. By itself, as a gasdynamic/mechanical driving mechanism, sympathetic coupling between chamber wall oscillatory motion and the internal flow within the motor chamber can lead to substantial pressure wave growth.^{3,4} In the present investigation, a number of different chamber vibration scenarios (axial, radial, and tangential oscillation cases) are numerically evaluated as a baseline for further work.

NUMERICAL MODEL

For the purposes of the present investigation, treatment of the internal motor flow as a non-reactive, non-conducting, unsteady, viscous compressible fluid at a high chamber gas pressure and temperature is appropriate at this stage of evaluation. The authors are primarily interested in establishing the level of pressure wave growth within the flow due to mechanical vibration. Previous work⁵ by the first author utilized a quasi-one-dimensional explicit Godunov-type solver (random-choice method) for numerically simulating a number of forced and free motor vibration cases. In the current effort, the CFD-ACE+ code⁶ by CFD Research Corporation, utilizing a comprehensive multi-physics implicit finite-volume solver, is applied for the solution of two-dimensional flow models and associated wall motion. For some of the work done in

this study, the wall structure does not require finite-element modeling via the FEMSTRESS module of the ACE+ code, given that a forced rigid-body wall motion prescribed for a specified sinusoidal displacement and frequency satisfies the driving requirements on the internal flow. Where static and/or dynamic structural deformation is a factor influencing internal flow behaviour, the FEMSTRESS module is employed.

COMPUTATIONAL SETUP

Two dimensional computational domains and associated grids used in this analysis are shown in Figure 1(a,b,c).

Axial Disturbance. Boundary displacements are specified on surrounding walls, horizontal displacement following the sinusoidal

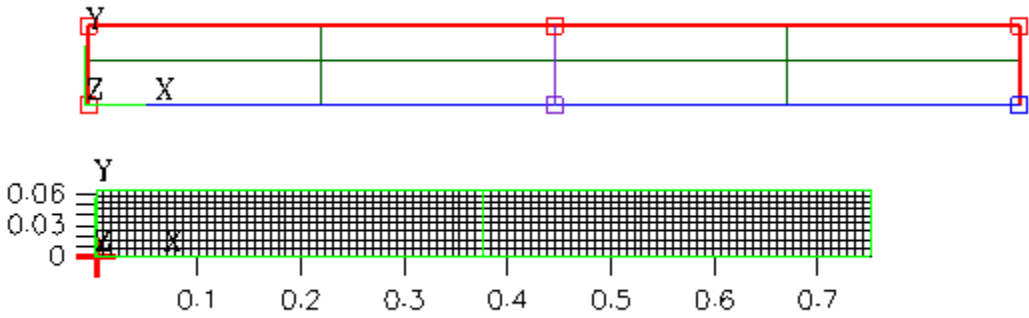


Figure 1a Computational Setup and Grid for Axial Disturbance
 Displacement function: $f(x)=0.002\sin(4273T)$, Ideal Gas law, mol.weight-26, visc= $8.1E-5$ kg/m-s,
 15000 time steps, time step $t=1.5E-6$ sec, Pinit= 9400000 Pa

Radial Disturbance. Boundary displacement is specified for upper wall ($y=0.25$ m), radial displacement following the sinusoidal

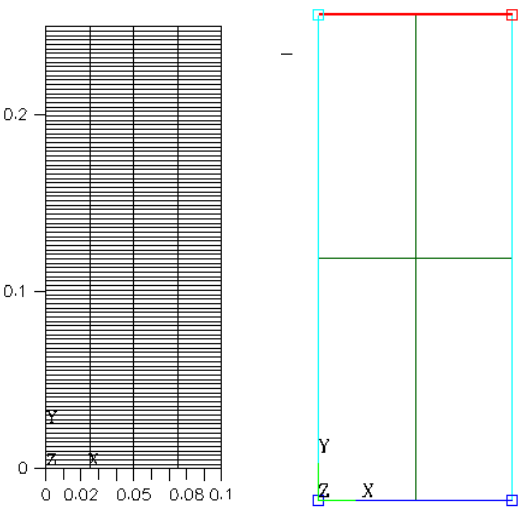


Figure 1b Computational Setup and Grid for Radial Disturbance
 Displacement function $f(y)=4.45E-5\sin(16336T)$, Mol.weight =22, visc= $8.07E-5$ kg/m-s,
 300,000 time steps , time step $t=1.875E-7$ sec

Tangential Disturbance. Boundary displacements are specified on the surrounding wall, horizontal displacement following the sinusoidal

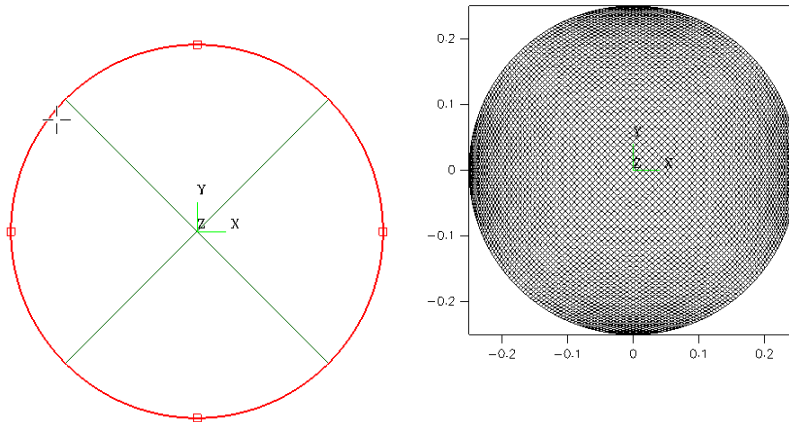


Figure 1b Computational Setup and Grid for Tangential Disturbance

Displacement function $f=1.84E-4\sin(7854T)$, mol weight=22, visc = $8E-5$ kg/m-s, 160,000 steps, time step $t=5E-7$ sec

NUMERICAL RESULTS AND DISCUSSION

The first motor chamber evaluated is a simple two-dimensional, axisymmetric duct with closed walls at each end, with a typical propellant gas at a chamber gas temperature of 3000 K. For this cold-flow evaluation, mass input from some portion of the bounding wall representing propellant gas injection, and a corresponding exhaust flow exiting through a choked nozzle at one end, while able to be modeled in the ACE+ code, are not required. A simple sinusoidal prescribed forcing function is applied for the motion of the end walls, essentially representing an axial rigid-body structural vibration scenario. The effective resonant driving frequency is 680 Hz for this 0.75 m long duct, a value somewhat lower than the fundamental acoustic estimate of 720 Hz, with a peak displacement of 2 mm. This lower frequency value may in part be a function of the relatively coarse grid used for this evaluation. The internal pressure and axial velocity profiles 22.5 ms after initiation of vibration are provided in **Fig. 2**.

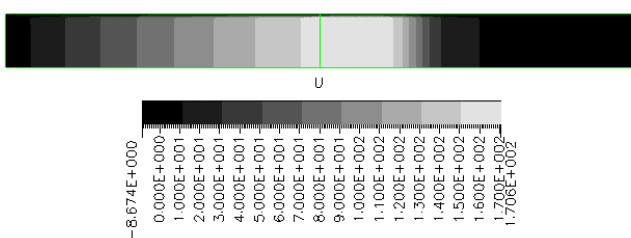


Figure 2a Axial velocity Distribution

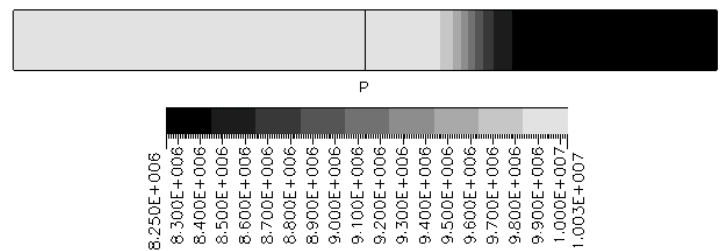


Figure 2b Internal Pressure Distribution

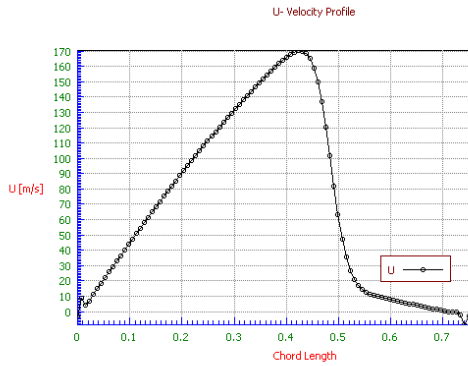


Figure 2c Axial Velocity Profile

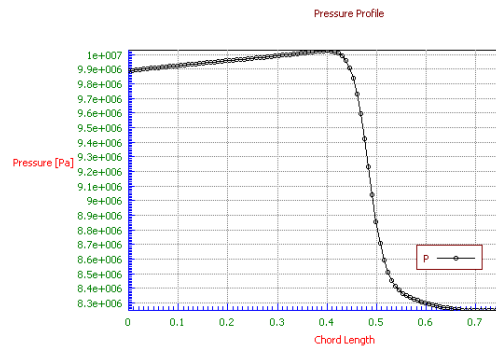


Figure 2d Pressure distribution profile

The baseline chamber pressure was 9.4 MPa at initiation (and the flow quiescent), and the wave development at the later time is substantial for the ± 3700 g acceleration being applied. This is further evidenced by the left-end pressure-time profile of **Fig. 3**, where one can see the limiting end-wall pressure wave is approaching a peak-to-trough strength of 4 MPa, with at least a portion of the wave having a steep shock front. This result is comparable to that reported for an earlier, one-dimensional study.³

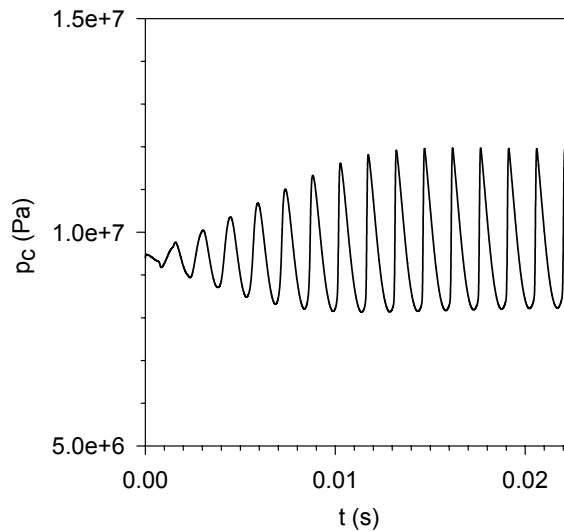


Figure 3 Left-wall pressure-time profile

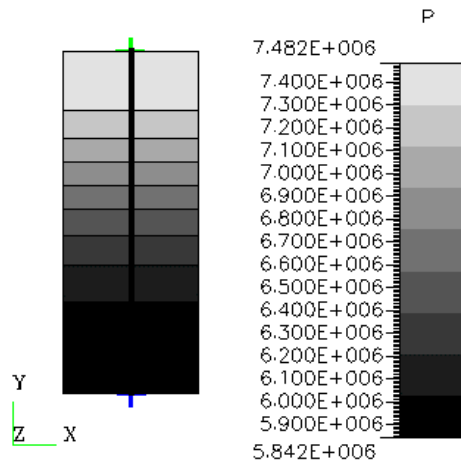


Figure 4a Pressure Distribution Profile

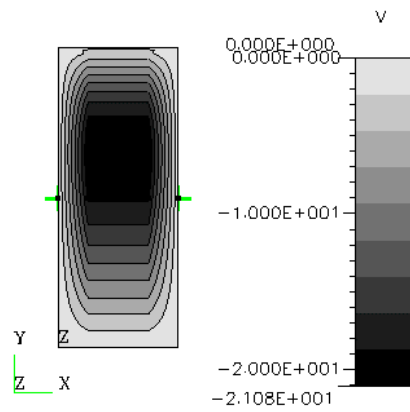


Figure 4b Radial Velocity V Distribution Profile

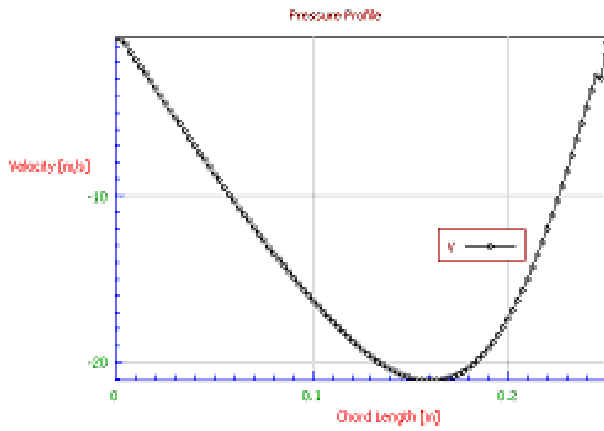


Figure 4c Radial Velocity V Distribution Profile

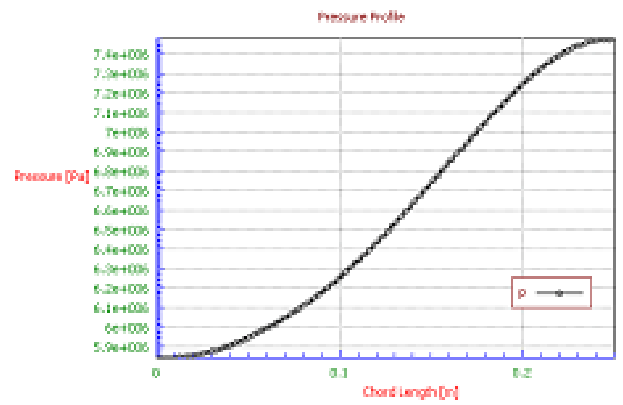


Figure 4d Pressure Distribution Profile

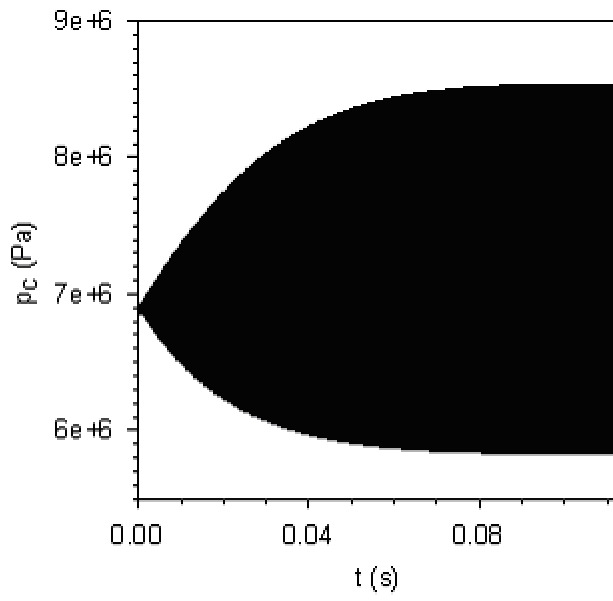


Figure 5. Cavity Centerline pressure-time profile

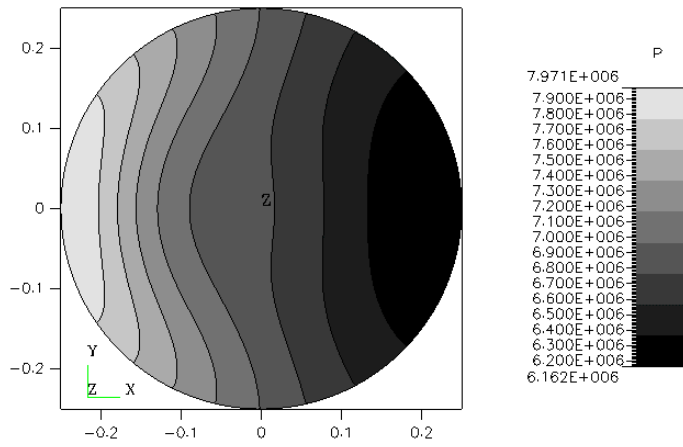


Figure 6 a Internal Pressure

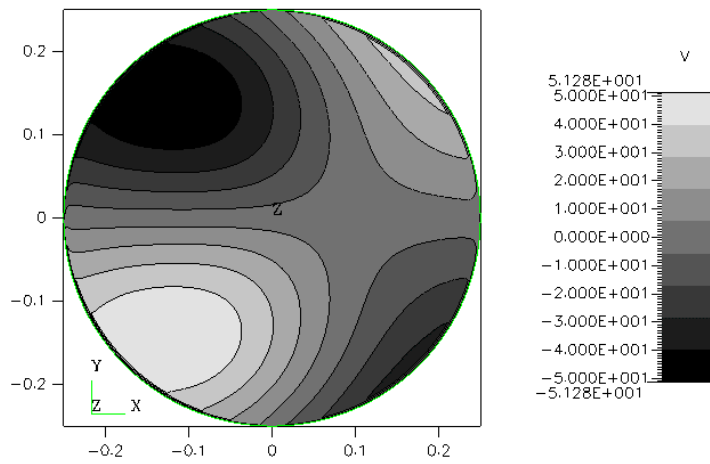


Figure 6d. Lateral Velocity (V) Profile

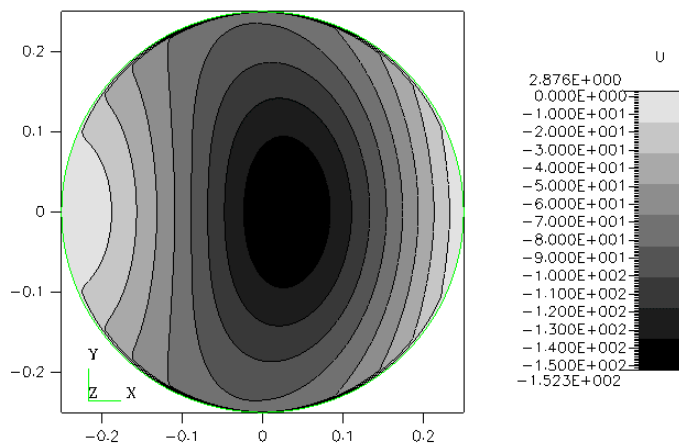


Figure 6d. Horizontal velocity U profile

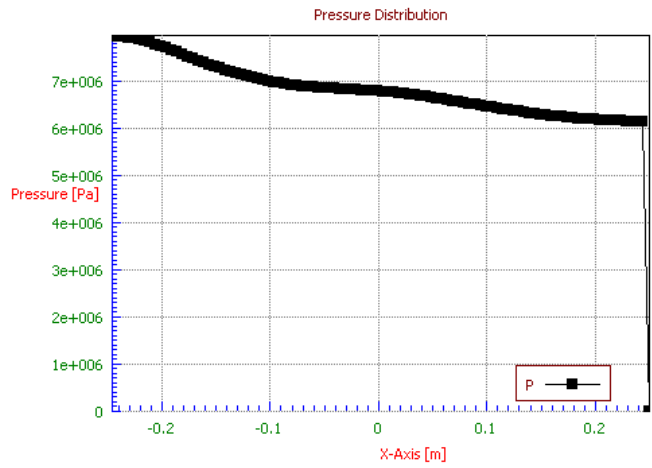


Figure 6 d Pressure Distribution along X-axis

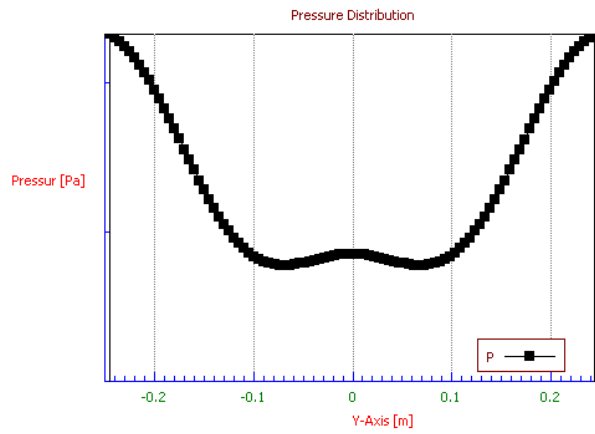


Figure 6 d Pressure Distribution along Y-axis

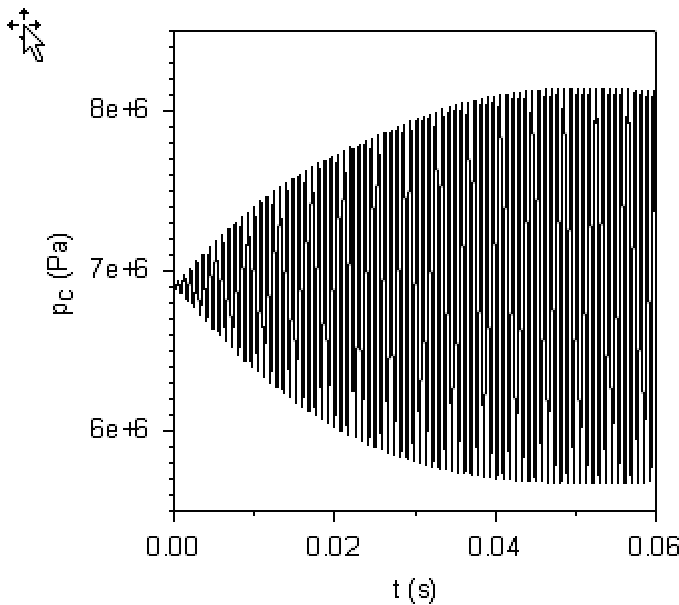


Figure 7. Right-wall pressure-time profile

The second motor chamber scenario involves a two-dimensional axisymmetric section (0.25 m radius, with a short axial length) having its peripheral wall vibrate in the radial direction. Again, the analysis in this case does not require mass input from the bounding walls, and with two closed walls at the left and right ends of the chamber section, there is no axial throughflow. The effective resonant driving frequency is 2600 Hz, a value somewhat lower than the nominal 2905-Hz acoustic fundamental radial frequency. The peak radial displacement of the wall is 0.045 mm, producing a peak acceleration value of 1200 g. The internal pressure and radial velocity profiles 0.1125 s after initiation of vibration are provided in **Fig. 4**, noting that the baseline pressure was 6.9 MPa in this case. The peak pressure wave magnitude occurs at the centreline of the chamber section, approaching 3 MPa at later times as evidenced in **Fig. 5**. This limiting value is somewhat lower than that reported in the quasi-one-dimensional study of Ref. 4 (on the order of 5 to 15 MPa on a fluctuating peak wave strength). A number of runs at progressively higher grid densities and smaller time steps with the current numerical model suggests a limiting magnitude that is asymptoting towards the Ref. 4 levels. The resonant driving frequency of Ref. 4 was 2895 Hz and corresponding acceleration was ± 1500 g, which would also account for the current results being somewhat lower in strength. The strength of the pressure wave at the peripheral wall is substantially less, approaching a value of about 1.2 MPa, as compared to a value of about 3 MPa reported in Ref. 4. The proportional strengths of the centreline and wall values are however comparable.

The third motor chamber scenario involves looking at a two-dimensional lateral section of a motor chamber with a 0.25 m radius, and having the section move side-to-side in a fundamental tangential rigid-body vibration mode. As before, there is no mass input from the surrounding walls. While the fundamental acoustic estimate is 1430 Hz, the effective resonant driving frequency is in the vicinity of 1250 Hz with the current numerical model and grid density. With a maximum tangential displacement of 0.182 mm, the resulting peak acceleration level is about 1100 g. The internal pressure and horizontal/lateral velocity profiles

80 ms after initiation of vibration are illustrated in **Fig. 6**, noting that the baseline pressure in the chamber section was 6.9 MPa. The peak pressure wave magnitude occurs at the left and right end walls of the chamber section. With the numerical grid density employed, a peak wave strength of about 2.5 MPa is predicted as may be seen in **Fig. 7**, while at the chamber centre, the limiting wave strength is about 0.8 MPa. The peak value reported in Ref. 4 is on the order of 5 MPa, while at the chamber centre, the wave strength is on the order of 1.6 MPa. As before, the proportional strengths of the waves at the two locations are comparable between the two studies. The resonant driving frequency was 1430 Hz in Ref. 4, delivering a higher acceleration level of 1500 g, which can account for some of this difference in limiting magnitudes (as before, increasing grid density and smaller time steps also tended to increase the values seen in the current study). In addition, the appearance of a twin-wavelet front to the cyclic wave suggests that the driving frequency in the current study was not quite at resonance, so that would also result in a lower limiting wave magnitude. Finally, the appearance of peaking at double the fundamental frequency, at the cavity centre, is in evidence, in agreement with the earlier study.

A final scenario illustrating free structural vibration (including structural deformation) is considered. A shock-tube setup for testing the structural response of a solid propellant grain (surrounded by a thin aluminum casing and thicker steel sleeve) to shock wave passage is a proposed means of experimentally collecting information pertinent to solid rocket motor combustion instability studies. The righthand side of the tube containing the core section of inert solid propellant, is initially pressurized (step loaded) from ambient atmospheric pressure to 10.5 MPa at $t = 0$, with the chamber gas temperature at 3000 K. The radial displacement profile of the structure at $t = 0.097$ ms is presented in **Fig. 8**. The result of the structural deflection can be seen on the flow by the radial velocity profile and local Mach number profile, at the same time, shown in **Figs. 9** and **10**. The resulting static pressure profile over time at the midlength centreline position of the righthand tube section is provided in **Fig. 11**, and the corresponding radial deflection of the propellant inner surface and outer sleeve surface at the midlength position is illustrated in **Fig. 12**. Pressure wave amplitudes are on the order of 5% of the base pressure at the tube centreline, produced by the cyclic movement of the propellant surface primarily, but affected as well by the diaphragm movement upon pressurization (the diaphragm separates the left and right sections of the overall tube). In an actual experiment, this wave motion would need to abate before proceeding with rupturing the diaphragm to instigate a shock wave passage from the diaphragm station.

CONCLUDING REMARKS

The characteristic behaviour of axial and transverse waves appearing in a cylindrical combustor cavity have been described, for the case of prescribed structural vibration as the driving mechanism. It is apparent that at substantial vibration levels, there is the potential for a corresponding development of pressure waves at significant amplitudes. For partially unreacted flows in the motor chamber, one might expect even higher limiting wave magnitudes than that predicted in this investigation, given an enhanced, wave-coupled mixing and combustion process therein.

With the prescribed forced vibration results seen in this short study, and the simple shock-tube pressurization free vibration results provided as a final example, one has a baseline for further, more comprehensive work involving free structural vibration, with coupled fluid-structure modeling. For example, an initial pulse-induced axial shock wave moving down a combustor duct will induce a sequential development of radial structural vibration in the surrounding structure, producing local transverse waves that might play a factor in gasdynamic or combustion processes (the arrival of the axial shock at the head or nozzle end of the motor chamber will induce axial vibration that may also play a role in wave activity). The resonant frequencies of the structure can be expected to influence the development (or hindrance) of resonant wave activity in the internal gas cavity.

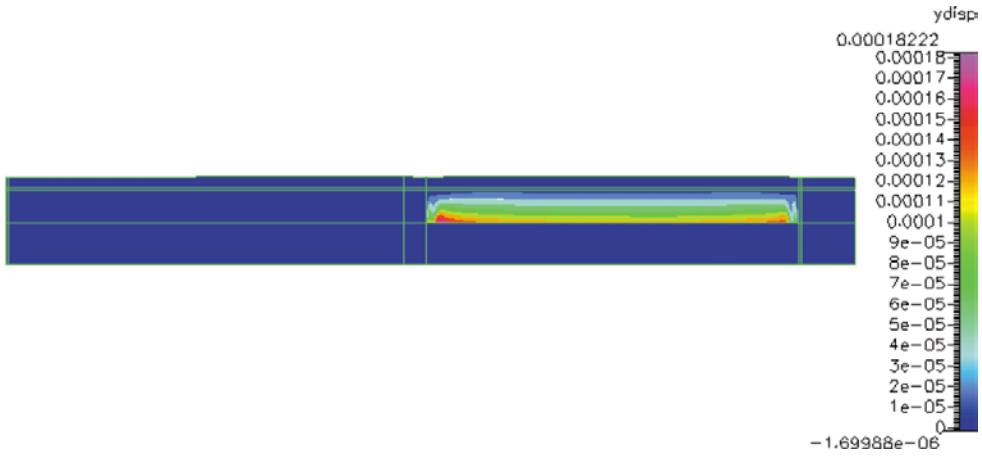


Figure 8. Radial Displacement Profile

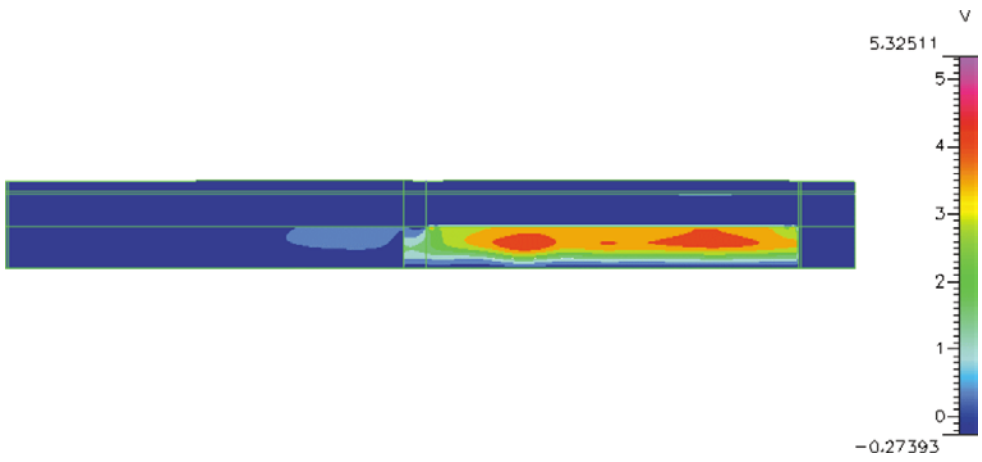


Figure 9. Radial velocity Profile

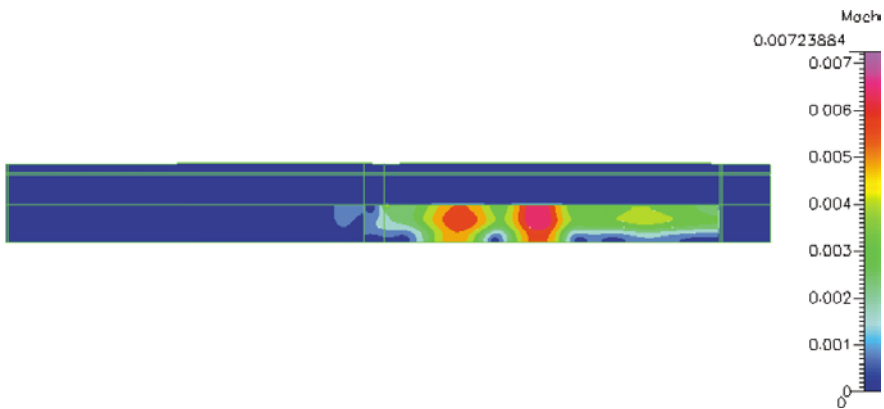


Figure 10. Local Mach Number distribution

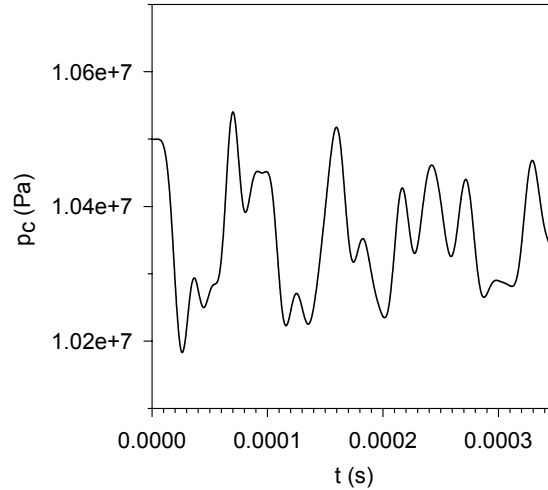


Figure 11. Centerline Pressure-time profile

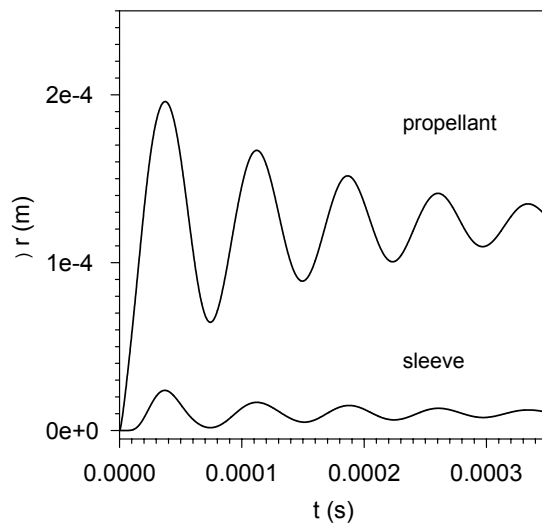


Fig. 12 Deflection of propellant surface and sleeve external wall

REFERENCES

1. Huzel, D.K. and Huang, D.H., "Modern Engineering for Design of Liquid-Propellant Rocket Engines," *Progress in Astronautics and Aeronautics*, Vol. 147, American Institute of Aeronautics and Astronautics, Washington D.C., 1992.
2. Harris, P.G., Wong, F.C. and de Champlain, A., "The Influence of Structural Vibrations on Pulse-Triggered Nonlinear Instability in Solid Rocket Motors: An Experimental Study," AIAA Paper No. 96-3250, July 1996.

3. Greatrix, D.R., "Axial Motor Vibration and Associated Internal Ballistics," AIAA Paper No. 97-3337, July 1997.
4. Greatrix, D.R., "Transverse Vibration and Rocket Combustor Internal Ballistics," AIAA Paper No. 97-3338, July 1997.
5. Greatrix, D.R. and Gottlieb, J.J., "Higher-Order Random-Choice Method for Internal Ballistic Flows," proceedings of the 7th Annual Conference of the CFD Society of Canada, pp. 9-15 – 9-20, May 1999.
6. Singhal, A.K., "Key Elements of Verification and Validation of CFD Software," AIAA Paper No. 98-2639, June 1998.